

Numerical Analysis of First and Second Cycles of Oxyhydrogen Pulse Detonation Engine

Soshi Kawai* and Toshi Fujiwara†
 Nagoya University, Nagoya 464-8603, Japan

In the present study, numerical analysis of pulse-detonation-engine (PDE) cycles such as combustion, exhaustion, and fuel-injection phases is performed. A numerical scheme that is second-order accurate in time and space, MacCormack-total-variation-diminishing scheme, was used to solve the Navier–Stokes equations, where a simplified two-step chemical reaction model is introduced. The dependence of fuel-injection time on 1) the opening width of intake port, 2) reservoir pressure, and 3) injection angle is studied. Through the numerical analysis of PDE-cycle operation, the time required for each phase is estimated for each model PDE; the dependence on PDE tube length and the time required for PDE operation are studied. The performances (such as impulse and thrust density) of four straight model PDEs that have different tube lengths are estimated and compared with the theoretical result of Endo–Fujiwara analysis. The useful formula for impulse per unit area, which is similar to the expression in the theoretical analysis, is derived from the numerical analysis.

Introduction

A DETONATION phenomenon is the interaction between a front-running shock wave and subsequent coupled combustion, generating a high pressure and temperature that is basically uncontrollable in comparison with conventional flames. The direction of research has mostly been prevention of or protection from hazard.

For several years, however, there has been a trend to control detonation propagation and to utilize its high power and high-density energy in positive directions like pulse detonation engine (PDE)¹; Eidelman and Grossmann reignited the study of PDE. Pulse-detonation-engine research has spread widely recently because it is considered a good candidate for an aerospace propulsion system of the next generation.²

The operational principle of PDE can be explained briefly in the following. As a simple example, a rocket-engine-type PDE operation of cylindrical shape is considered. The cycle operation of PDE consists of the four phases, which are fuel supply, ignition, combustion, and exhaustion. As shown in Fig. 1, a mixture of hydrogen fuel and oxygen is supplied into PDE, followed by the ignition of mixture by an igniter placed over the closed upstream end. The combustion wave is accelerated to a detonation and propagates downstream in PDE. Thereafter, the detonation wave is emitted from PDE exit, with the burned gas being exhausted. By repeating such four phases, PDE generates thrust.

One-dimensional numerical and theoretical analyses of PDE have been performed by numerous workers^{3–6} without considering injection phase and diffusive transport processes (viscosity, heat conductivity, and diffusion). In one-dimensional analysis, furthermore, it is difficult to treat fuel injection and mixing process, which are the longest time-consuming processes during PDE operation. Two-dimensional numerical analyses of PDE also have been performed by some workers.^{7,8} In these studies, however, diffusive transport processes and fuel injection in PDE operation were not considered.

In studying PDE, a key issue would be how to generate a Chapman–Jouguet (CJ)/quasi-CJ detonation in a short distance and how to realize high-frequency operation. Therefore, investigation of fuel injection and subsequent ignition has become unavoidable and important.

In the present work, a two-dimensional cycle analysis of PDE containing an Ar-diluted stoichiometric oxyhydrogen mixture is performed. To achieve a high-frequency-running engine, we pay attention specifically to the exhaustion and injection process for the second cycle, where the burned gas generated in the first cycle still remains within PDE. A second-order MacCormack-total-variation-diminishing (TVD) scheme is used to solve Navier–Stokes equations where a simplified two-step chemical reaction model⁹ is introduced.

Mathematical Model and Numerical Method

Governing Equations and Numerical Method

The governing equations are two-dimensional Navier–Stokes ones, containing the mass-conservation equations for two progress variables α (induction reaction) and β (exothermic reaction):

$$\frac{\partial U}{\partial t} + \frac{\partial E}{\partial x} + \frac{\partial F}{\partial y} = \frac{\partial E_v}{\partial x} + \frac{\partial F_v}{\partial y} + S \quad (1)$$

where

$$U = \begin{pmatrix} \rho \\ \rho u \\ \rho v \\ e \\ \rho \beta \\ \rho \alpha \end{pmatrix}, \quad E = \begin{pmatrix} \rho u \\ \rho u^2 + p \\ \rho uv \\ (e + p)u \\ \rho \beta u \\ \rho \alpha u \end{pmatrix}, \quad F = \begin{pmatrix} \rho v \\ \rho uv \\ \rho v^2 + p \\ (e + p)v \\ \rho \beta v \\ \rho \alpha v \end{pmatrix}$$

$$E_v = \begin{pmatrix} 0 \\ \tau_{xx} \\ \tau_{xy} \\ u\tau_{xx} + v\tau_{xy} - q_x \\ \rho D_\beta \frac{\partial \beta}{\partial x} \\ 0 \end{pmatrix}$$

Received 15 March 2002; revision received 6 March 2003; accepted for publication 7 May 2003. Copyright © 2003 by Soshi Kawai and Toshi Fujiwara. Published by the American Institute of Aeronautics and Astronautics, Inc., with permission. Copies of this paper may be made for personal or internal use, on condition that the copier pay the \$10.00 per-copy fee to the Copyright Clearance Center, Inc., 222 Rosewood Drive, Danvers, MA 01923; include the code 0001-1452/03 \$10.00 in correspondence with the CCC.

*Graduate Student, Department of Aerospace Engineering; kawai@flab.eng.isas.ac.jp. Student Member AIAA.

†Professor, Department of Aerospace Engineering.

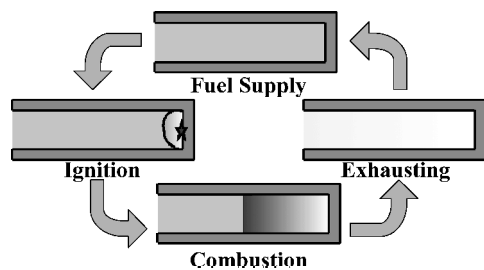


Fig. 1 Operational principle of PDE.

$$F_v = \begin{pmatrix} 0 \\ \tau_{yx} \\ \tau_{yy} \\ u\tau_{yx} + v\tau_{yy} - q_y \\ \rho D_\beta \frac{\partial \beta}{\partial y} \\ 0 \end{pmatrix}, \quad S = \begin{pmatrix} 0 \\ 0 \\ 0 \\ 0 \\ \rho w_\beta \\ \rho w_\alpha \end{pmatrix}$$

This set of coupled nonlinear differential equations describes the conservation of density ρ , momentum $\rho v = (\rho u, \rho v)$, energy e , and two progress variables $\rho\alpha$ and $\rho\beta$. To close this set of equations, the pressure is defined as

$$p = (\gamma - 1)[e - \rho\beta Q - 0.5\rho(u^2 + v^2)] \quad (2)$$

where γ and Q are the specific heat ratio of gas and the exothermic energy. The auxiliary relations among dependent variables are given by the thermal equation of state for a perfect gas $p = \rho RT$; τ_{ij} , q_i , and D_β denote shear-stress tensor, heat-flux vector, and diffusion coefficient.

The two progress variables α and β are explicitly given in the following.

α (induction reaction):

$$w_\alpha \equiv \frac{d\alpha}{dt} = -\frac{1}{\tau_{\text{ind}}} = -k_1\rho \exp\left(-\frac{E_1}{RT}\right)$$

where τ_{ind} denotes the chemical induction time.

β (exothermic reaction):

$$w_\beta \equiv \frac{d\beta}{dt} = \begin{cases} 0 & (\alpha > 0) \\ -k_2\rho^2 \left\{ \beta^2 \exp\left(-\frac{E_2}{RT}\right) \right. \\ \left. -(1-\beta)^2 \exp\left(-\frac{E_2+Q}{RT}\right) \right\} & (\alpha \leq 0) \end{cases}$$

In the modified Korobeinikov-Levin chemical model the rate constants k_1 , k_2 , E_1 , and E_2 are adjusted to agree, regarding its chemical induction time and temperature profile, with Oran's elementary reaction model¹⁰ as much as possible.

A numerical scheme, that is second-order accurate in time and space, MacCormack-TVD scheme, where transport terms (viscosity, heat conductivity, and diffusion) are evaluated as additional terms by the central differencing, was used to solve the just-mentioned Navier-Stokes equations.

Model PDE and Initial Condition

The present model PDE is a straight two-dimensional detonation channel with its upstream end closed, having two open ports at upper and lower PDE walls for injecting an oxyhydrogen mixture ($2\text{H}_2 + \text{O}_2 + 7\text{Ar}$), while the downstream end is open for exhausting a burned gas, as shown in Fig. 2. Our PDE runs under the ground

Table 1 Model PDE configuration

Case	PDE width W , mm	PDE length L , mm
a	30.0	100.0
b	30.0	200.0
c	30.0	300.0
d	30.0	400.0

Table 2 Effect of resolution on calculated cell size

Test grid	Square-shape mesh size, μm	Cell size, cm	Ratio between calculated and experimental cell size
1	200.0	N/A	N/A
2	150.0	0.75	1.53
3	100.0	0.6	1.22
4	67.0	0.6	1.22
5	50.0	0.6	1.22

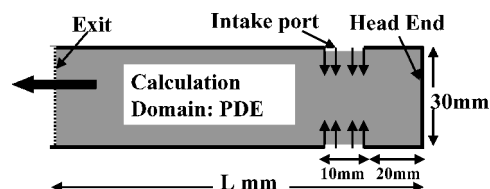


Fig. 2 Calculation domain of model PDE.

condition at $P_{\text{env}} = 1.0$ atm. The computations are performed for four different PDEs that have same width ($W = 30$ mm) and different lengths (L), as listed in Table 1. The first cycle starts after an oxyhydrogen mixture is filled up in PDE under the initial pressure $P_1 = 1.0$ atm and temperature $T_1 = 298.15$ K.

Boundary Condition

Because calculation domain is limited only inside PDE, the boundary condition utilized at the open end is derived from the method of characteristics. This ensures no constraints imposed on the flow quantities when the outflow is supersonic, whereas it is subjected to the required constraints when the flow becomes subsonic, so that the influence of environment comes into play only through the pressure at tube end for subsonic flow conditions. This specified pressure boundary condition at PDE exit is considered to have some influence on the inner solution because of the subsonic flow character at exit. Miyasaka et al.⁷ evaluated such influence by computing between the two cases, with and without outer space of PDE. According to Ref. 7, such influence is found to be very small, indicating that an environment pressure set to the pressure boundary of PDE exit for a subsonic outflow is a good approximation. In this analysis, the specified pressure boundary condition was applied to PDE exit.

The PDE wall boundary condition is assumed to be nonslip, adiabatic, and noncatalytic. The inflow boundary condition at intake ports is assumed to be a choked flow where the inflow Mach number is kept at 1.0 and the fixed pressure P_r and temperature T_r are both given.

Resolution/Mesh Convergence

It is known in numerical analysis of detonation that the physical properties obtained from calculation are highly dependent on grid resolution and numerical scheme. The resolution is upgraded as much as possible by testing five different grids. The effect of grid resolution on cell size is shown in Table 2 at the initial pressure 0.5 atm and temperature 298.15 K, which yielded the experimental cell size $\lambda = 0.49$ cm obtained by Strehlow.¹¹

As seen in Table 2, the cell size does not change when the square-shape mesh size becomes less than 100 μm . Furthermore, in comparison with the experimental cell size $\lambda = 0.49$ cm, grids 3–5 uniformly give $\lambda = 0.6$ cm ($1.22 \times$ experimental λ), reasonably close to the experimental cell size, whereas the combustion wave does not

accelerate up to a detonation for grid 1 and grid 2 giving $\lambda = 0.75$ cm ($1.53 \times$ experimental λ). Twenty-percent discrepancy with experiment is the converged result of our simplified two-step chemical reaction model calculation. Our two-step reaction model, however, is adjusted to agree with Oran's elementary reaction model as much as possible. Thus, we have concluded that grid 1 and 2 resolution is not enough, whereas grids 3–5 are reliable to provide PDE-cycle analysis including performance estimation, but not that the detailed behaviors of unsteady shock-boundary-layer interaction are not resolved by this mesh convergence. Based on these results, the present analyses are carried out using grid 3, where the square-shape mesh size is $100 \mu\text{m}$. Thus, the total grid number is $(L \times 10) \times 300$ ($\Delta x = \Delta y = 100 \mu\text{m}$).

Results and Discussion

Numerical Analysis of First Cycle

Combustion Process

Ignition in the first cycle has already been performed by assuming a CJ detonation obtained from one-dimensional analysis. To generate a two-dimensional detonation, the initial one-dimensional detonation starting from the closed upstream end is disturbed by placing inhomogeneities near the side walls, which act like a Shchelkin wire. The one-dimensional CJ detonation is perturbed into a two-dimensional detonation in a short deflagration-to-detonation transition (DDT) distance, propagating toward downstream end. Thereafter, the detonation front leaves the channel, followed by burned gas exhaust from the channel; at the instant when the head-end pressure $P_h = P_{env} (= 1.0 \text{ atm})$, the fresh mixture starts flowing from the intake ports into the second cycle.

The pressure distribution in PDE (case a) at $10.8, 31.3,$ and $50.6 \mu\text{s}$ after ignition is shown in Fig. 3. Figure 4 shows the change of pressure distribution along PDE (case a) center axis during evolution of combustion process after ignition. The detonation structure of

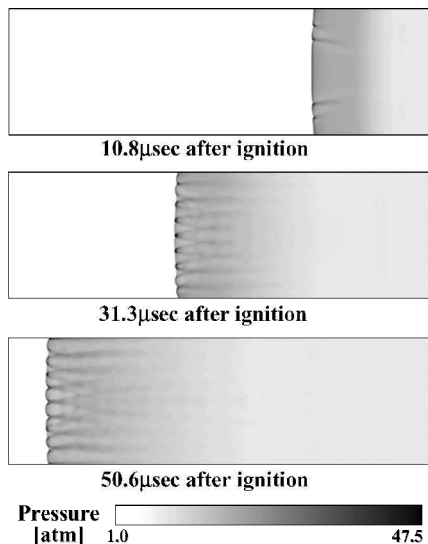


Fig. 3 Pressure distribution in PDE (case a) after ignition.

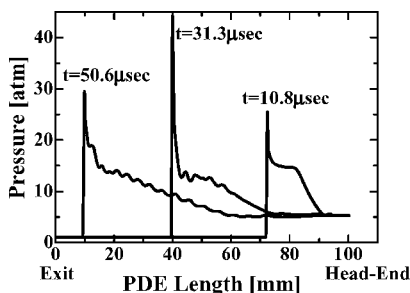


Fig. 4 Combustion evolution along PDE (case a) center axis after ignition.

having triple points immediately after ignition is formed, and the features that the detonation wave has propagated downstream in PDE are observed. The propagation velocity of the detonation front is shown in Fig. 5, where the calculated velocity during 100-mm traveling (case a) during the first cycle is found close to the CJ value. In addition, there is essentially no difference among the four cases under consideration. During the combustion process in the first cycle, detonation propagates toward the downstream end immediately after ignition. The pressure distribution snapshot (case a) and distribution of pressure and temperature (case a) along the PDE center axis, at the instant when detonation front has reached PDE exit ($56.2 \mu\text{s}$ after ignition), are shown in Figs. 6 and 7. The calculated time required for combustion process among four model PDEs (cases a–d) is $56.2, 119.8, 183.6,$ and $247.1 \mu\text{s}$, respectively.

Exhaust of Combustion Products

The history of pressure and temperature at the center of intake port and head-end, until immediately before the fresh oxyhydrogen intake ports are opened up, is shown in Figs. 8 and 9. At this valve opening time the head-end pressure is equal to the environment pressure ($P_h = P_{env} = 1.0 \text{ atm}$). By the time when fuel injection starts from two intake ports, the pressure at intake ports has become 0.98 atm while the temperature stays at 1270 K . Because the detonation velocity is very close to CJ value $U = 1591 \text{ m/s}$, the time for detonation to leave PDE length 100 mm [case a] is $t = 56.2 \mu\text{s}$; at $t \leq 56.2 \mu\text{s}$, therefore, the detonation front is still barely inside PDE. Figure 9 indicates that the pressure history can be divided into two distinct stages, as pointed out by Kailasanath³: 1) a plateau starting from $t \geq 0.0 \mu\text{s}$, giving the pressure $P_p/P_{CJ} = 0.38$, that

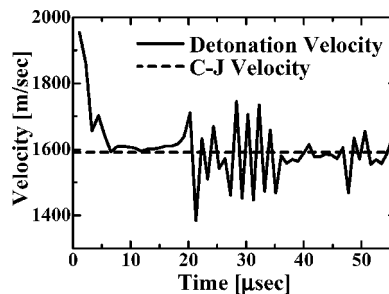


Fig. 5 Temporal variation of detonation velocity.

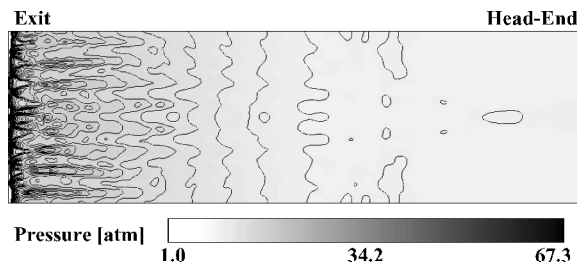


Fig. 6 Pressure contour (case a) at instant when the detonation front has reached exit.

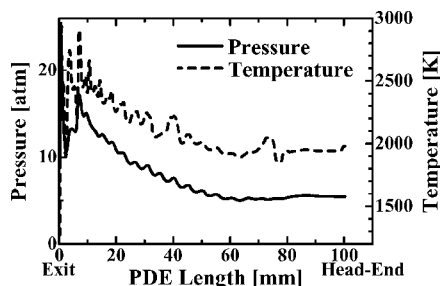


Fig. 7 Distribution of pressure and temperature (case a) along PDE center axis.

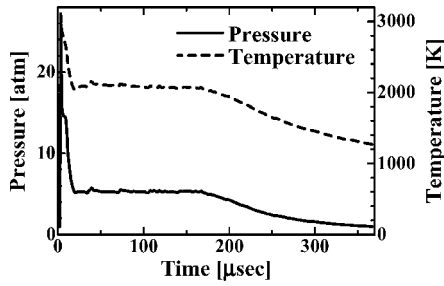


Fig. 8 Evolution of pressure and temperature at center of intake port (case a).

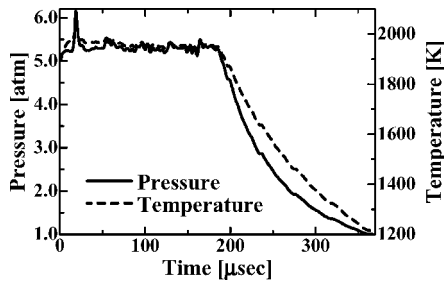


Fig. 9 Evolution of pressure and temperature at head end (case a).

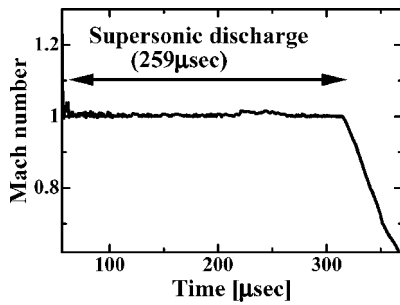


Fig. 10 Evolution of Mach number at center of PDE exit (case a).

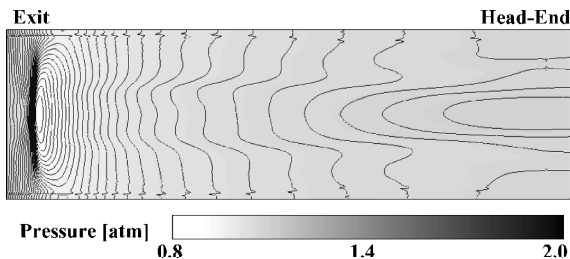


Fig. 11 Pressure contour (case a) immediately before fresh oxyhydrogen intake ports are opened up.

is, $P_p = 5.27$ atm ($P_{C1} = 13.86$ atm), which lasts for a long time $0.0 \mu s \leq t \leq 187.8 \mu s$; 2) a relaxation $187.8 \mu s \leq t \leq 367.1 \mu s$ down to a low-pressure $P_h/P_{env} = 1$. This plateau pressure is the primary part to generate thrust of PDE. Figure 10 gives the history of Mach number at the center of PDE exit. With regard to the flow at PDE exit, its Mach number is kept always at 1.0 from the start of exhaust until $259.1 \mu s$ later, indicating that the exit flow is choked. Thereafter, the flow at PDE exit decreases down to subsonic.

The pressure distribution snapshot (case a) and the distribution of pressure and temperature (case a) along PDE center axis at the instant immediately before the fresh oxyhydrogen intake ports are opened up ($367.1 \mu s$ after ignition, and $P_h = P_{env} = 1.0$ atm), are shown in Figs. 11 and 12. Figure 13 shows the change of pressure distribution along center axis, at several times during the pressure relaxation process in PDE (case a); the time is now counted from the start of exhaust. Figure 13 indicates that the burned gas

Table 3 Specific impulse I_{sp} for four cases

Case	I_{sp}, s
a	6576
b	6651
c	6702
d	6747

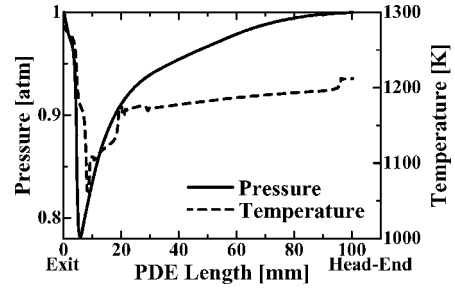


Fig. 12 Distribution of pressure and temperature (case a) along PDE center axis, at the instant when oxyhydrogen intake ports are opened up.

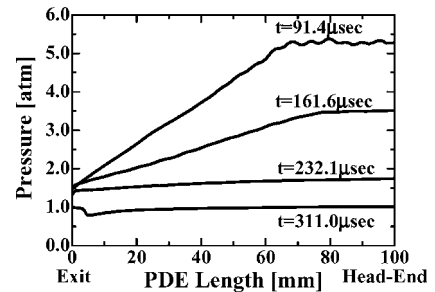


Fig. 13 Pressure relaxation process along PDE (case a) center axis.

from the first cycle exhausts quickly from PDE open end, where the pressure decrease in PDE is influenced by the environmental pressure. The calculated times required for exhaust process among four model PDEs (cases a–d) are $311.0, 626.7, 950.7,$ and $1289 \mu s$, respectively.

Next, the specific impulse based on oxyhydrogen fuel is estimated from the history of head-end pressure P_h minus initial pressure of mixture $P_1 (= 1.0$ atm), as follows:

$$I_{sp} = \frac{[\text{impulse per unit length during 1 cycle}]}{[\text{filled fuel mass per unit length}]} \quad (3)$$

$$= \frac{\int_0^W \int_0^{t_{env}} (P_h - P_1) dy dt}{\int_0^W \int_0^L \rho_1 g dy dx}$$

where $W, \rho_1,$ and g denote the width of PDE, filled fuel density, and acceleration of gravity, while t_{env} is the time elapsed until $P_h = P_{env}$ is realized. Cartesian coordinates system x and y are the length and width directions.

The specific impulse I_{sp} for four cases acquired from formula (3) is shown in Table 3. Although a slightly increasing tendency of specific impulse is seen for longer tubes, we can derive a general conclusion that I_{sp} is independent of PDE length as long as DDT distance is assumed zero. The temporal behavior of impulse (case a) per unit depth is shown in Fig. 14; the asymptotic limit of impulse (case a) is set to 3.16 N/s/m to define the one-cycle time t_{env} . Note here that the impulse per unit depth is proportional to PDE length L , as shown in Fig. 15.

Next, we try to compare the results of numerical analysis, using a figure on impulse per unit area, first proposed by Kailasanath¹² on the basis of one-dimensional numerical analysis, as is shown in Fig. 16. The impulse obtained by Kailasanath one-dimensional analysis is proportional to the product of t_{C1} defined by $L(\text{PDE length})/D_{C1}$ and the pressure difference $P_p - P_1$, where D_{C1} is the

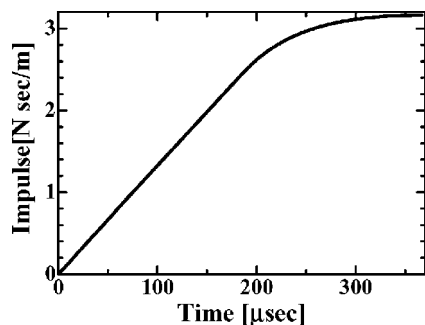


Fig. 14 Evolution of impulse per unit depth (case a).

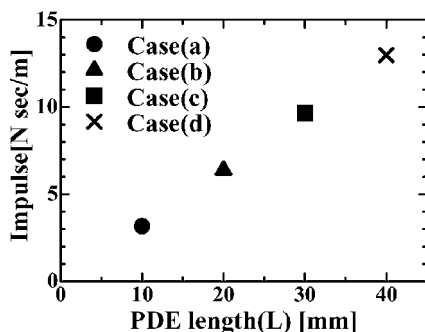


Fig. 15 Impulse compared among four model PDEs (cases a-d).

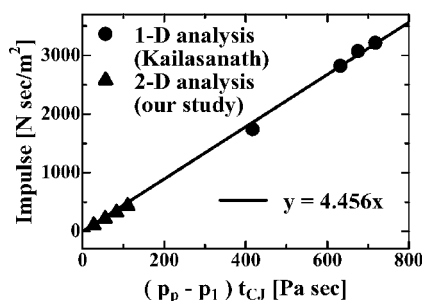


Fig. 16 Impulse curve of Kailasanath one-dimensional analysis compared with our two-dimensional results.

CJ velocity. Interestingly, our results of two-dimensional analysis also lie on the same straight line. The impulse per unit area is given by the following equation:

$$I/A = 4.456(P_p - P_1)t_{CJ} \quad (4)$$

This equation about impulse per unit area derived from numerical simulations is also similar to the expressions from theoretical analysis.^{5,6}

Numerical Analysis of Second Cycle

Immediately after the head-end pressure P_h has decreased down to the environmental pressure P_{env} , a fresh oxyhydrogen mixture is injected into PDE, which still contains a high-temperature burned gas, by opening two intake ports.

Size effect of intake port is tested by locating a port specifically at the center of PDE head end, where the open ratio = intake port width/PDE width = 1.0 ~ 0.17, where the port is connected to a reservoir tank of $P_r = 10.0$ atm and $T_r = 298.15$ K. Fuel-injection time was calculated after the intake port opens until the value of β at the PDE exit plane attains 1.0. It means that unburned fuel mixture has arrived at the PDE exit. The pressure and temperature around intake port is $P_i = 1.0$ atm and $T_i = 1212$ K. The relation between calculated fuel-injection time and open ratio is shown in Fig. 17; when the open ratio becomes smaller, the fuel-injection time sharply increases, indicating the existence of proper value.

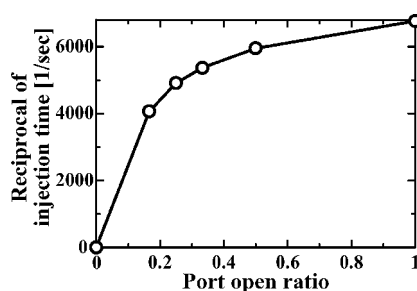


Fig. 17 Relation between calculated injection time and port open ratio.

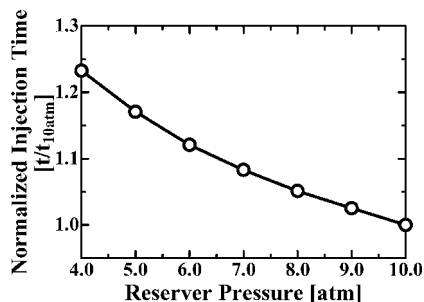


Fig. 18 Relation between calculated injection time and reservoir pressure.

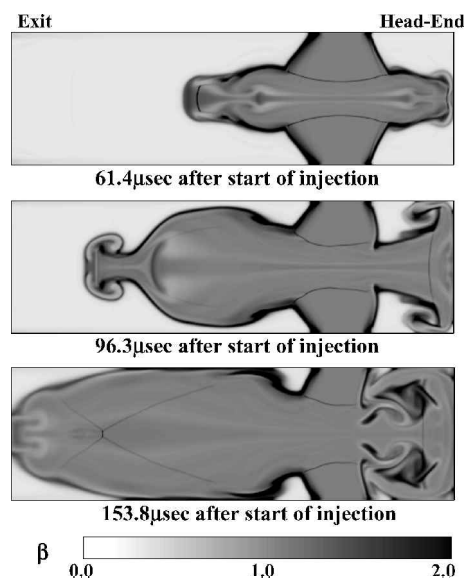


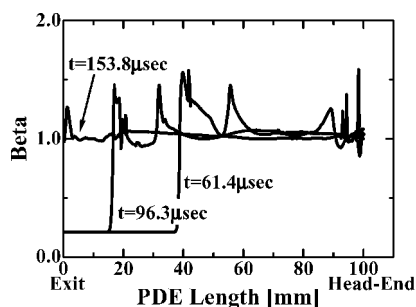
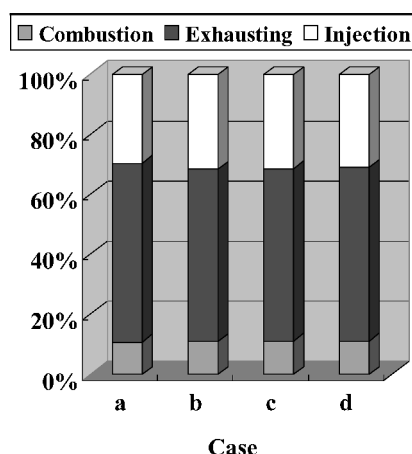
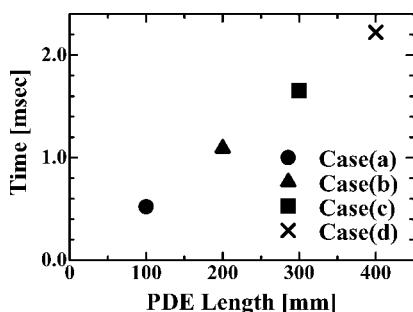
Fig. 19 The β distribution in PDE (case a) after start of fuel injection.

Next, the effect of reservoir pressure is tested for a model PDE (case a), as shown in Fig. 2. Normalized fuel-injection time (injection time/injection time for reservoir pressure 10 atm) for different reservoir pressures in case a is compared, where the reservoir pressure P_r is changed between 10 and 4 atm. Figure 18 shows that the calculated fuel-injection time is a decreasing function of the reservoir pressure, as is easily expected; the difference is only 23% for the pressure change $P_r = 10 \sim 4$ atm. We performed an analysis to find out dependence of injection angle on fuel-injection time (not shown in this paper). The injection angle analyzed for the four cases is leaned in the direction of PDE exit 60, 45, 30, and 0 deg from the right-angle direction to the surface of PDE wall; no influence is seen to fuel-injection time. In conclusion, the fuel-injection time depends only on 1) intake port width and 2) reservoir pressure P_r .

Henceforth, the fuel-injection time is studied for four model PDEs connected to the $P_r = 10.0$ atm reservoir tank at $T_r = 298.15$ K (fuel injection is right angled to wall), where the performance of four model PDEs is also calculated. The β distribution in PDE (case a) at 61.4, 96.3, and 153.8 μs after starting of injection is shown in Fig. 19.

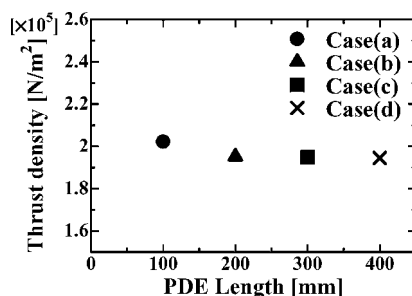
Table 4 Time for each process in one cycle for four model PDEs (cases a–d)

Case	a		b		c		d	
	Second	%	Second	%	Second	%	Second	%
Combustion	5.62×10^{-5}	10.8	1.20×10^{-4}	11.0	1.84×10^{-4}	11.1	2.47×10^{-4}	11.1
Exhausting	3.11×10^{-4}	59.7	6.27×10^{-4}	57.4	9.51×10^{-4}	57.5	1.29×10^{-3}	58.0
Injection	1.54×10^{-4}	29.5	3.46×10^{-4}	31.6	5.19×10^{-4}	31.4	6.88×10^{-4}	30.9
One cycle	5.21×10^{-4}	100	1.09×10^{-3}	100	1.65×10^{-3}	100	2.22×10^{-3}	100

**Fig. 20** Distribution of β along PDE (case a) center axis at different times after start of injection.**Fig. 21** Percentage of each process for four model PDEs (cases a–d).**Fig. 22** Time needed for one cycle of model PDEs (cases a–d).

By injecting an oxyhydrogen mixture from two intake ports during the second cycle, the features of fuel expansion and diffusion are observed. The distribution of β along PDE (case a) center axis after starting fuel injection is shown in Fig. 20; β is about 1.0 (unburned mixture) nearly everywhere in PDE behind the contact surface. The general features of fuel injection can be understood from Figs. 19 and 20. The calculated times required for injection process among four model PDEs (cases a–d) are 153.8, 345.6, 518.8, and 687.5 μ s, respectively.

The times required for combustion, exhaust, fuel injection, and cycle completion for cases a–d are shown in Table 4. The ratio

**Fig. 23** Thrust density of four model PDEs (cases a–d).

between each process and complete cycle is also shown as % in Table 4. As another representation of Table 4, a bar graph on percentage of each process is given in Fig. 21, whereas the time to complete PDE one cycle is given in Fig. 22; note that the ratio of the time required for each process in one cycle (combustion, exhaust, and fuel injection) does not depend on PDE length, that is, ratio of the time required for each process is fixed though the length of PDE changes. Moreover, the one cycle time can easily be estimated if the PDE length and reservoir pressure P_r are both given; it is closely proportional to PDE length as shown in Fig. 22.

The thrust density of each model PDE (cases a–d) is given in Fig. 23, showing that it is again independent of PDE length; a fixed thrust density is essentially obtained. The obtained thrust density of our model PDEs ($195,000 \text{ N/m}^2$) is very high compared with a general turbojet value (for example, $31,200 \text{ N/m}^2$), and even better than a general ramjet value (for example, $176,700 \text{ N/m}^2$). In general, as mentioned earlier, the performance of model PDE has no dependence on PDE length, but depends on 1) the initial conditions, 2) intake port width, and 3) reservoir pressure P_r .

Conclusions

In this study a two-dimensional analysis of PDE two-cycle operation is performed for four different PDE lengths, where we pay attention specifically to the behaviors of 1) burned gas exhaust and 2) oxyhydrogen injection during the second cycle and performance estimation.

1) During the first cycle, the detonation propagation and subsequent slow pressure relaxation process inside PDE are simulated under the ground condition. It is confirmed that the flow at PDE exit plane becomes choked during exhaust process, indicating that the process is essentially a one-dimensional flow.

2) The impulse per unit depth increases in proportion to PDE length L . The impulse given by the present two-dimensional analysis shows a well fitting with a straight line originally delivered by Kailasanath one-dimensional analysis. Note that the straight line is similar to the expressions from theoretical analysis.

3) When the open ratio (intake port width/PDE width) becomes smaller, the fuel-injection time increases sharply. Fuel-injection time is a decreasing function of the reservoir pressure as is easily expected. However, the difference is only 23% for the pressure change $P_r = 10 \sim 4 \text{ atm}$. Change of injection angle has not influenced the fuel-injection time at all. Thus, the fuel-injection time is dependent only on the reservoir pressure and intake port width.

4) The time ratios among elementary processes (combustion, exhaust, and fuel injection) are independent of PDE length. Moreover, the one-cycle completion time can easily be estimated if the PDE

length and reservoir pressure are both given; the cycle time is closely proportional to PDE length.

5) The thrust density, the most important performance indicator of PDE, is nearly independent of PDE length, in the case of zero-DDT distance assumption.

References

¹Eidelman, S., and Grossmann, W., "A Review of Propulsion Applications of the Pulsed Detonation Engine Concept," AIAA Paper 89-2446, July 1989.

²Roy, G., "Review of Recent Developments in Combustion and Detonation Research," AIAA Paper 2001-0473, Jan. 2001.

³Kailasanath, K., "A Review of PDE Research-Performance Estimates," AIAA Paper 2001-0474, Jan. 2001.

⁴Fujiwara, T., Fukiba, K., and Miyasaka, T., "Efficiency Study of PDE Based on Quasi-One-Dimensional Calculation of Detonation, Chemical Physics Reports," *Journal of the Russian Academy of Science*, Vol. 20, No. 6, 2001, pp. 99–104.

⁵Endo, T., and Fujiwara, T., "A Simplified Analysis on a Pulse Detonation Engine Model," *Transactions of the Japan Society for Aeronautical and Space Science*, Vol. 44, No. 146, 2002, pp. 217–222.

⁶Endo, T., and Fujiwara, T., "Analytical Estimation of Performance Parameters of an Ideal Pulse Detonation Engines," *Transactions of the Japan*

Society for Aeronautical and Space Science. Vol. 45, No. 150, 2003, pp. 249–254.

⁷Miyasaka, T., Fujiwara, T., Endo, T., Zhang, F. Y., and Matsuo, T., "Estimation of Pulse Detonation Engine Performance Using a Two-Dimensional CFD Analysis Based on Detailed Oxyhydrogen Chemistry," *Journal of the Japan Society for Aeronautical and Space Sciences*, Vol. 50, No. 586, 2002, pp. 10–15.

⁸Chiping, Li, and Kailasanath, K., "Performance Analysis of Pulse Detonation Engines with Partial Fuel Filling," AIAA Paper 2002-0610, Jan. 2002.

⁹Korobeinikov, V. P., Levin, V. A., Markov, V. V., and Chernyi, G. G., "Propagation of Blast Waves in a Combustible Gas," *Astronautica Acta*, Vol. 17, 1972, pp. 529–537.

¹⁰Oran, E., Young, T., and Boris, J., "Application of Time-Dependent Numerical Methods to the Description of Reactive Shocks," *Seventeenth Symposium (International) on Combustion*, Combustion Inst., Pittsburgh, PA, 1979, pp. 43–54.

¹¹Strehlow, R. A., "Gas Phase Detonation: Recent Developments," *Combustion and Flame*, Vol. 12, 1968, pp. 81–101.

¹²Kailasanath, K., "Recent Developments in the Research on Pulse Detonation Engines," AIAA Paper 2002-0470, Jan. 2002.

M. Sichel
Associate Editor